

Regional downscaling for stable water isotopes: A case study of an atmospheric river event

Kei Yoshimura,^{1,2} Masao Kanamitsu,³ and Michael Dettinger^{3,4}

Received 8 February 2010; revised 5 May 2010; accepted 11 May 2010; published 23 September 2010.

[1] In this paper an isotope-incorporated regional model is developed and utilized for simulations of an atmospheric river event that occurred in March 2005. A set of sensitivity experiments and comparisons with observations confirm that the kinetic isotopic exchange between falling droplets and ambient water vapor below the cloud base was mostly responsible for the initial enrichment and subsequent rapid drop of the deuterium abundance in precipitation observed during the event even under humid conditions. According to the budget analysis the increase in isotopic composition during the latter half of the event was primarily due to horizontal advection. The contribution of condensation from different atmospheric heights to the ground precipitation was not reflected in the precipitation isotopes.

Citation: Yoshimura, K., M. Kanamitsu, and M. Dettinger (2010), Regional downscaling for stable water isotopes: A case study of an atmospheric river event, *J. Geophys. Res.*, 115, D18114, doi:10.1029/2010JD014032.

1. Introduction

[2] The composition of stable water isotopes in precipitation and tropospheric water vapor is basically controlled by water's phase changes, so that the atmospheric processes associated with the water's phase changes may be deduced from the isotopic signals. For this reason, water isotopes are regarded as useful natural tracers of atmospheric hydrologic processes. To understand the spatiotemporal distribution mechanism of the isotopes in precipitation and water vapor, various types of direct measurements have been made all over the world [Dansgaard, 1964; Rozanski *et al.*, 1993; Clark and Fritz, 1997]. In addition, the recent spectroscopy technique makes instant measurement of the isotopic composition of water vapor possible using ground-based instruments [Schneider *et al.*, 2010] and satellite-onboard remote sensors [Frankenberg *et al.*, 2009]. However, measurements of isotopes with high temporal resolution have been limited, primarily owing to lack of resources, and such data are indeed precious.

[3] Recently, Coplen *et al.* [2008] (hereafter C08) have reported a series of precipitation isotopic composition data in 30-min resolution associated with an "atmospheric river" (AR) event. An AR is characterized by a narrow band of strong horizontal water vapor fluxes concentrated in the lower troposphere immediately ahead of polar cold fronts

[Ralph *et al.*, 2004]. The mechanism of an AR is particularly important since the precipitation affected by it contributes significantly to annual precipitation over the western United States. The data showed a remarkable variation of isotopes; that is, rain that was enriched in deuterium in the beginning of the event underwent a sudden drop of deuterium abundance within an hour and became enriched again within a single sequential rain event that lasted for 12 h. The study concluded that the isotopic variation reflected the precipitation temperature, so that the signal can be attributed to the height of the precipitation generation: The deuterium-enriched rain in the very beginning was generated by a shallow and warm cloud, and the sharp drop in δD was associated with a transition from shallow to deep cloud when a synoptic-scale ascent occurred. Deuterium and ^{18}O abundances in water vapor decrease when adiabatic condensation associated with an uplifting of air mass occurs. This process is known as Rayleigh distillation for isotopic fractionation.

[4] Although this interpretation is straightforward, the mechanism is perhaps too simple and it digresses from rather classical points of view such as those of Ehhalt *et al.* [1963]. For example, even when the cloud is deep and generates condensate at a high and cold altitude, some contribution from deuterium-enriched water vapor in the lower part of the cloud should still remain. Moreover, some reports point out the possible isotopic exchange between falling raindrops and surrounding vapor below the cloud base [Friedman *et al.*, 1962; Miyake *et al.*, 1968; Stewart, 1975; Gedzelman and Arnold, 1994], which may increase the isotope ratio.

[5] In this study we try to numerically simulate the isotopic and meteorological variations and investigate the mechanism of the isotopic variation. An isotope-incorporated atmospheric general circulation model [e.g., Yoshimura *et al.*, 2008] is generally suitable for this type of problem, but

¹Atmosphere and Ocean Research Institute, University of Tokyo, Tokyo, Japan.

²Also at Japan Agency for Marine-Earth Science and Technology, Yokosuka, Japan.

³Scripps Institution of Oceanography, University of California, San Diego, La Jolla, California, USA.

⁴Also at U.S. Geological Survey, La Jolla, California, USA.

since the target variations are within 12 h with 30 min resolution, the global model resolution (i.e., more than 100 km; typically 200 km) is too coarse. Therefore, we incorporated the isotopes into a regional model and ran it with a sufficiently high resolution to simulate the meteorology and the isotopic variation.

[6] For a good simulation of stable water isotopes in precipitation, initial conditions and lateral boundary conditions are as important as they are in short-range weather prediction [Yoshimura *et al.*, 2003, 2004; Sturm *et al.*, 2005]. Until recently there was no good four-dimensional isotope data set suitable for real-data simulation. The recently completed 30 year reanalysis-“nudged” isotope-incorporated AGCM simulation by Yoshimura *et al.* [2008] was found to be very useful for this type of study. Several direct comparisons between the data set and isotope measurements revealed that the data set is accurate enough to serve as an alternative to water isotope assimilation analysis [Abe *et al.*, 2008; Uemura *et al.*, 2008; Schneider *et al.*, 2010]. We used this data set as a boundary condition and initial state of the newly developed isotopic regional model.

[7] The following section describes the target AR event and the new isotopic regional model. The simulation design including the lateral boundary condition and specification of the spectral nudging technique is also noted. In section 3 the simulation results are presented and the main processes that drive the isotopic variation of the AR event are investigated. Section 4 contains the summary and conclusions.

2. Data and Method

2.1. Observations

[8] Isotopic and meteorological observation data were taken from C08. The meteorological observatories are located at Bodega Bay (BBY; 38.34°N, 123.06°W) and Cazadero (CZD; 38.61°N, 123.22°W), and the 30 min interval precipitation samples were taken at CZD. In the very beginning of the rain event, the δD of precipitation was about -25% , but it suddenly decreased to about -80% within an hour. It kept this low δD value for about 4 h and then increased to -20% within 3 h. After this the composition very gradually decreased down to -30% over the next 3 h until the rain event ended. We note that the Next Generation Weather Radar (NEXRAD) National Mosaic Reflectivity Images (available at <http://www4.ncdc.noaa.gov/cgi-win/wwcgi.dll?WWNEXRAD~IMAGES2>) are also used for verification of the model-simulated precipitation distribution.

2.2. Isotopic Regional Spectral Model (IsoRSM)

[9] The isotopic species for water vapor (HDO and $H_2^{18}O$) have been added as tracers in the latest version of the Scripps Experimental Climate Prediction Center’s regional spectral model (RSM; Kanamitsu *et al.* [2005]). The major nonisotopic physical processes include convective parameterization (the relaxed Arakawa-Schubert scheme [Moorthi and Suarez, 1992]), land surface (Noah land surface model [Ek *et al.*, 2003]), radiation (Chou scheme [Chou and Suarez, 1994]), and a planetary boundary scheme (Hong and Pan, 1996)]. Thanks to extensive efforts by the previous developers, the RSM is regarded as a major regional

climate model and it has been used in many multimodel intercomparison studies [e.g., Miller *et al.*, 2009].

[10] The isotopic processes are identical to those in the isotopic global spectral model (IsoGSM [Yoshimura *et al.*, 2008]). These processes are based on the thermodynamic equilibrium fractionation among vapor, liquid, and ice based on Majoube [1971a, 1971b] for most of the phase transition and on kinetic fractionation for surface evaporation from open water [Merlivat and Jouzel, 1979], for condensation from vapor to ice under supersaturation conditions at temperatures lower than -20°C [Jouzel and Merlivat, 1984], and for evaporation and isotopic exchange from liquid raindrop into unsaturated air [Stewart, 1975].

[11] The kinetic isotopic exchange associated with droplets’ evaporation is formulated by Stewart [1975] and implemented into the IsoRSM with forms of equations (1). It is noted that these equations are principally the same as those in Appendix A3 of Bony *et al.* [2008].

$$R_r = \varepsilon \left[(R_{r,0} - \gamma R_{v,0})(m/m_0)^\beta + \gamma R_{v,0} \right] + (1 - \varepsilon)R_{r,0},$$

$$R_v = [q'_0 + (m'_0 - mR_r)]/q,$$

$$\text{with } \begin{cases} \beta = \frac{1 - \mu}{\mu}, \\ \gamma = \frac{\alpha_e h_{\text{eff}}}{1 - \mu}, \\ \mu = \alpha_e (D/D')^n (1 - h_{\text{eff}}), \end{cases} \quad (1)$$

where m is the rain droplet volume; R_r and R_v are the isotopic ratios of rain droplets and ambient vapor; the subscript 0 indicates original values before the isotopic effect; α_e is the equilibrium isotope fractionation factor; D' and D are the molecular diffusivities of isotopic vapor and ordinary vapor [Merlivat, 1978]; n is a degree of freedom, which is assumed to be 0.58 [Gat, 2000], and h_{eff} is the effective relative humidity [Hoffman *et al.*, 1998], which assumes more humid conditions inside a cloud compared to a grid average humidity (h) with a factor of 1.4 and a maximum value of 100% ($h_{\text{eff}} = \max(1.4 \times h; 100\%)$); q' and m' denote the vapor volume and rain droplet volume of the isotopic species; and ε is the fraction of droplets reaching the isotopic equilibrium state. It is assumed that $\varepsilon = 45\%$ for convective clouds and $\varepsilon = 95\%$ for large-scale condensation, which captures the behavior that smaller drops equilibrate more rapidly [Hoffmann *et al.*, 1998]. These fixed fractions of the equilibrium state can be misleading since the residence time of droplets in a single model layer should vary dependent on the model layer’s thickness and droplet size distributions, which are dependent on rainfall rate, temperature, and humidity [Lee and Fung, 2008]. Therefore, we test a set of sensitivity experiments with different values of the equilibrium fraction as described in section 2.4.

[12] When the effective relative humidity (h_{eff}) is nearly 100%, the value of R_r is approximated from equation (1) as follows:

$$R_r \approx \varepsilon \alpha_e R_{v,0} + (1 - \varepsilon)R_{r,0}. \quad (2)$$

This indicates that the isotopic composition of the droplets becomes a linearly interpolated value between the equilib-

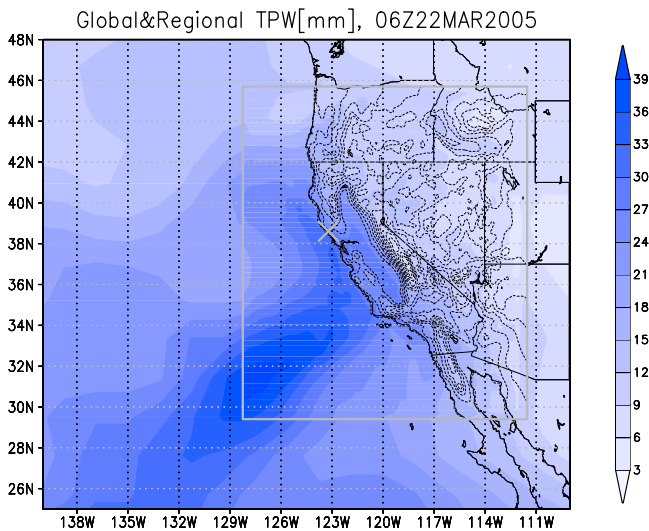


Figure 1. Domain of the regional downscaling experiments, shown by the rectangle outlined in gray. Dashed contours represent topography used, with 300 m intervals (0 m contour is omitted). Shades denote total precipitable water (TPW) distribution at 0600 UTC (or Zulu time) on 22 March 2005. The isotopic global spectral model (IsoGSM) simulated field is drawn outside the gray rectangle and the regionally downscaled field is drawn inside the rectangle. Location of the observation site, Cazadero (CZD), is shown by the cross.

rium fractionation state ($\alpha_e R_{v,0}$) and the nonfractionated state ($R_{v,0}$), dependent on ε .

[13] The RSM uses a spectral nudging technique [Kanamaru and Kanamitsu, 2007] to reduce large-scale bias in the dynamic field from the forcing fields in the regional model integration. The IsoRSM also adopts the improved spectral nudging proposed by Yoshimura and Kanamitsu [2009] and Kanamitsu *et al.* [2010], namely, (a) only the rotational part of the wind is used with slightly stronger nudging, (b) the area-averaged humidity is not corrected at all, and (c) the boundary zones are narrowed from 23% to 5% of the sides of the domain. It should be noted that isotopes and water vapor fields are not spectrally nudged or corrected, but forced by thinner lateral boundary zones, compared to other conventional lateral boundary nudging schemes [see Yoshimura and Kanamitsu, 2009].

[14] It is worthwhile to state that only two regional climate models with stable water isotopes exist. The first, REMO-iso, was developed by Sturm *et al.* [2005] from the European Centre Hamburg Model's Regional Model (REMO), and the second is the one in this study. Whereas studies with the REMO-iso have focused on regional climatology with long-term integration of the simulations [e.g., Sturm *et al.*, 2007], this study targets a case of very short-term synoptic-scale changes of the isotopic fields. This is indeed the first challenge, thanks to advancements in numerical techniques and resources (e.g., parallelized computing) and to better realization of synoptic features with spectral nudging and other previous physical and dynamical developments. In this study the isotopic parameterizations are tested for their applicability at such small scales.

2.3. Global Nudged Isotope Simulation Data

[15] Because of insufficient observational coverage of water isotopes, it has been difficult to perform a case study of regional simulation of water isotopes. However, recent work by Yoshimura *et al.* [2008] has made it possible to produce reasonably accurate synoptic-scale isotopic fields suitable for case study. They produced the large-scale analysis by using the global downscaling technique described by Yoshimura and Kanamitsu [2008] applied to a global atmospheric model with a water isotope process (data available at <http://meteora.ucsd.edu/~kyoshimura/IsoGSM1>). In this method the large-scale forcing was taken from National Centers for Environmental Prediction/Department of Energy (NCEP/DOE) Reanalysis 2 [Kanamitsu *et al.*, 2002], and water isotopes were fully predicted, including their sources and sinks, without utilizing any water isotope observations. Several validation studies of this analysis against limited observations showed that the analysis is sufficiently accurate for various process studies. We utilize this global analysis as the initial and lateral boundary conditions for this study.

2.4. Design of the Experiments

[16] An AR event that occurred on 21–22 March 2005 in northern California is selected for this study. Figure 1 shows the total precipitable water (TPW) from the global analysis for the isotopes. Because of the use of a global nudging method, this analysis is very similar to Reanalysis 2. A narrow band of precipitable water resembling a river-like feature, reaching from the tropical Pacific Ocean toward the western North American continent, is apparent. The target domain and resolution are 112°W–128°W, 25°N–48°N, and 10 km/28 σ levels, which match the California 50-Year Reanalysis Downscaling project of Kanamitsu and Kanamaru [2007]. The RSM has shown good performance over the western North American domain with 10 km resolution in previous studies. Therefore this study uses the identical domain and resolution. The U.S. Geological Survey's GTOPO30 (<http://edc.usgs.gov/products/elevation/gtopo30/gtopo30.html>) and land mask data sets are used to make the 10-km resolution topography (see Figure 1). A set of 10 day integrations from 0000 UTC, 15 March 2005, was performed. The time step for the model integration is 20 s. As already stated, the lateral boundary and initial conditions are taken from the global nudged isotope simulation, IsoGSM, and the surface boundary conditions, sea surface temperature and sea ice distribution, are the same as those used in NCEP/DOE Reanalysis 2. Simulation output is generated at hourly intervals and interpolated into 25 pressure levels in the vertical, that is, 1000, 975, 950, 925, 900, 875, 850, 825, 800, 775, 750, 725, 700, 650, 600, 550, 500, 450, 400, 350, 300, 250, 200, 150, and 100 hPa. All analyses in this paper are performed using these outputs unless noted otherwise.

[17] The set of experiments consists of the following. (1) CTL: A control run with all full isotopic processes. (2) E30: Same as CTL, but with a different equilibrium fraction for the large-scale condensation process; that is, 30% of droplets reach the equilibrium state instead of 95%. (3) NOF: Same as CTL, but no droplets (0%) reach equilibrium, so that no fractionation or isotopic exchanges occur during evaporation from droplets. (4) RAY: Instead of using Stewart's formulation, a simpler Rayleigh distillation for-

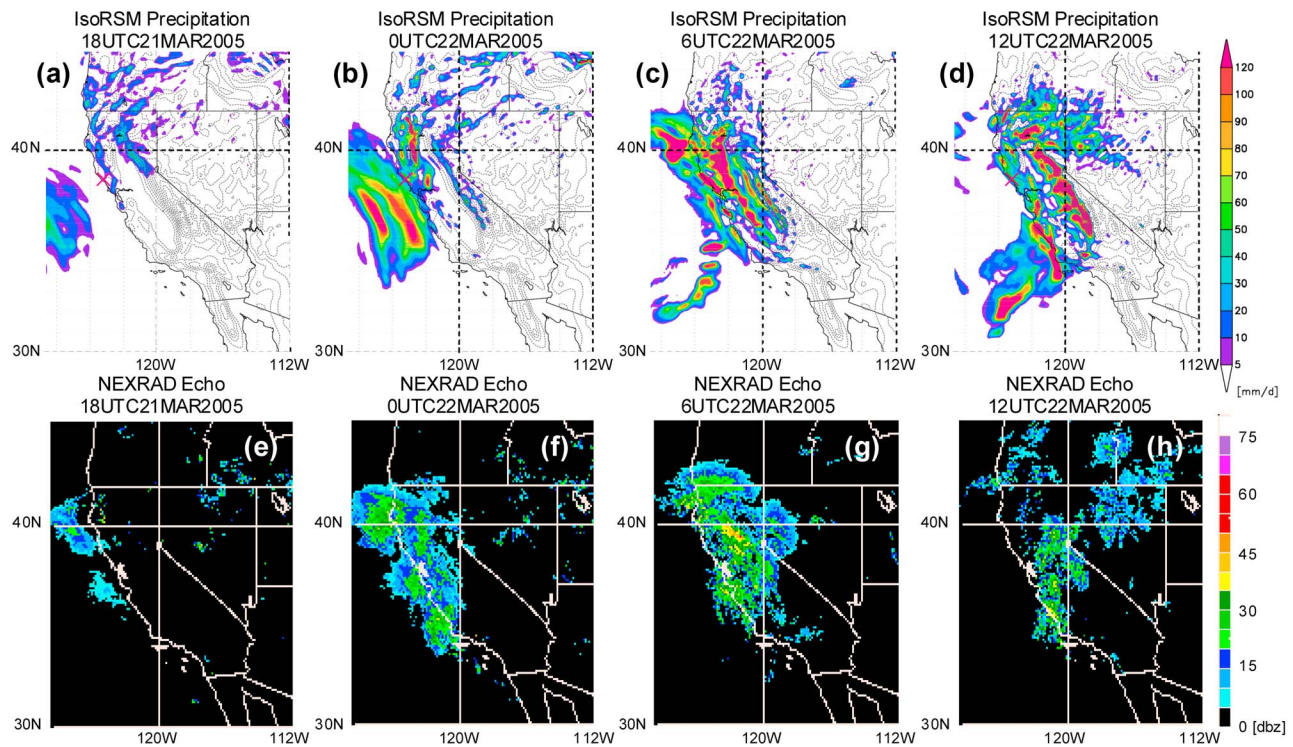


Figure 2. Precipitation fields from (a–d) the downscaling simulation and (e–h) radar observations (NEXRAD radar images). Vectors of the 10 m wind field are also shown in the simulation results. (e–h) Color bars indicate radar reflectivity (decibels; dbz) but not absolute amount of precipitation rate.

mulation is used for evaporation fractionation only. The equilibrium fraction parameter is the same as for the CTL, 95%.

[18] It should be noted that since heavy isotopes in water molecules do not interact with any model physical processes, changes in the isotopic processes do not affect the time evolution of other meteorological variables. These experiments simply aim at investigating how the isotopic composition over time is affected by the assumptions made during the phase change process under a fixed meteorological condition. As already noted, the initial and boundary conditions of the meteorological and isotopic fields are identical in all the experiments.

3. Results

3.1. Simulation of the Atmospheric River Event

[19] First, the IsoRSM’s ability to successfully simulate the western U.S. winter storm is examined. Figure 2 shows sequential snapshots of rainfall simulated by the model during the period, accompanied by Next Generation Weather Radar (NEXRAD) radar images. The eastward movement of the rainfall area and the most intense rainfall that occurred at 0600 UTC on 22 March over the northern Sierra Mountains (Figures 2c and 2g) are captured well by the model. However, there is a slight delay, about an hour, in the model’s eastward propagation of the rain area, and there is an overall overestimation of the rainfall amount, particularly over higher mountainous regions, although the observation is very uncertain over the complex topography.

[20] In Figure 3a the time series of the wind fields and humidity at BBY are shown in a form comparable to

Figure 2a in C08. There was a strong southerly low-level jet (LLJ) at the height of about 1 km mean sea level (MSL) from 0300 to 0800 UTC on 22 March, corresponding with the passage of a warm front followed by a cold front shown in Figure 2a. The LLJ is well reproduced in the simulation, but the wind speed is slightly weaker (the observed maxima are 28 m/s, whereas the simulated maxima are 24 m/s). In Figure 3b temporal variations of total precipitable water (TPW) and upslope wind component (directed from 230°) are plotted. The simulated TPW has some systematic overestimation, but the time variations are well reproduced (see Figure 2b in C08). The upslope wind speed is also nicely simulated, but the large increase from about 0000 to 0700 UTC is slightly less in the simulation, as expected from the weaker LLJ in Figure 3a.

3.2. Isotopic Simulations

[21] Figure 4 shows simulated and observed amounts of precipitation and deuterium composition (δD) at CZD. In accordance with the definition in C08, we also divide the rain event into five periods, namely, 2100 to 2300 UTC on 21 March (I), 2340 UTC on 21 March to 1000 UTC on 22 March (II), 1000 to 2300 UTC (III), 2300 to 0630 UTC (IV), and 0730 to 1000 UTC on 22 March (V). These periods correspond to the distinctive changes in isotopic composition in the model, namely, the beginning enrichment phase (I), sudden-drop phase (II), depletion phase (III), increase phase (IV), and ending enrichment phase (V), respectively. Although the period definition is taken from C08, it follows the simulated δD variation, so there are some differences from the C08 periods, mainly due to the blunter drop in δD in the beginning. Period I lasts a

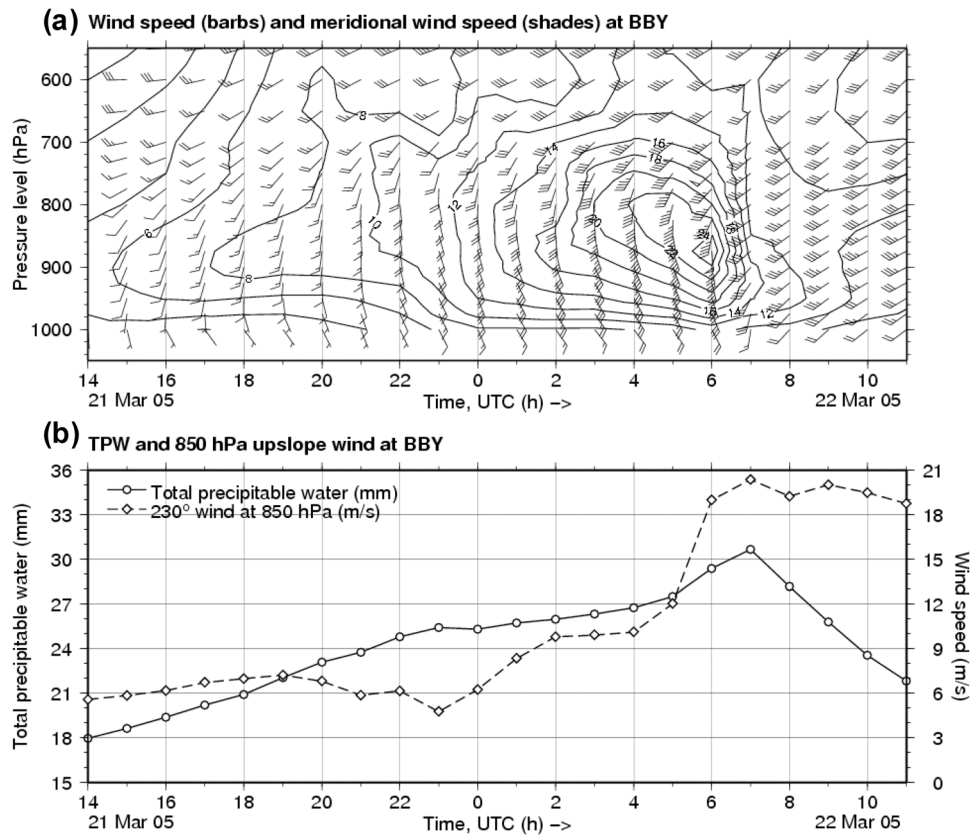


Figure 3. Simulated time sequences of atmospheric states at Bodega Bay (BBY; 38.34°N, 123.06°W) for (a) wind profiles (wind flags, 25 m/s; barbs, 5 m/s; half-barbs, 2.5 m/s) and meridional wind component (contours) and (b) upslope flow at 850 hPa (m/s; directed from 230°) and TPW (mm). Figures 3a and 3b are intentionally drawn to be directly comparable with Figures 2a and 2b of Coplen *et al.* [2008] (henceforth C08), respectively, but in the opposite horizontal direction.

little longer, period II starts a little later and lasts longer, and period III remains shorter. Periods IV and V correspond well to C08, and period VI is excluded from this study because it is after the passage of the cold front associated with the AR system.

[22] First, it is notable that the precipitation duration and variation were reasonably reproduced by the control simulation. The precipitation intensity stays low during periods I–III, suddenly increases during period IV, and drops in period V. Again, all of the sensitivity experiments in this study are designed to influence only the isotopic variables, so that all the experiments have the same precipitation variations. There is a somewhat significant overestimation in the amount of precipitation, as shown in Figure 2. This discrepancy may have a large impact on the isotopic simulation, so two additional experiments were performed: one with a different spectral nudging technique and another with a different initial condition. According to the results the precipitation amount is consistently overestimated, with small differences between the CTL and these two additional experiments (figures not shown). It is worthwhile to mention that the discrepancy may be due partly to the representativeness of the precipitation observation.

[23] Figure 4b shows the observed time series of the isotopic composition in precipitation and those of the

simulations. Among the sensitivity experiments the CTL performed the best, reproducing both the rapid drop (periods I–III) and the slight, gradual rise (periods IV and V) in the 12 h rain period. There seems to be a 1 h delay in the CTL δD variation compared to the observation. The reason for the delay is under investigation but presently there is no clear explanation. Furthermore, the control experiment underestimates the minima of δD in period III and keeps the underestimation for periods IV and V. This may be related to the precipitation overestimation throughout the event, but there may be other possible causes. For example, the δD value of the moisture from the lateral boundary might be too low, or the moisture supply from the surface could be too depleted of heavy isotopes. Since fixing these problems is beyond the scope of this paper, we leave the investigation into the possible causes of the δD underestimation and precipitation overestimation to further studies.

[24] All the other experiments degraded the δD variations in precipitation from the CTL. Interestingly, all the experiments show similar isotopic variations from 0300 UTC on 22 March 2008, when the non-bright-band precipitation (period IV) started to occur in reality (see Figure 3a in C08), and consequently, the precipitation intensity began to increase in both the simulation and reality (Figure 4a), but at the beginning of the event (periods I–III) there are large

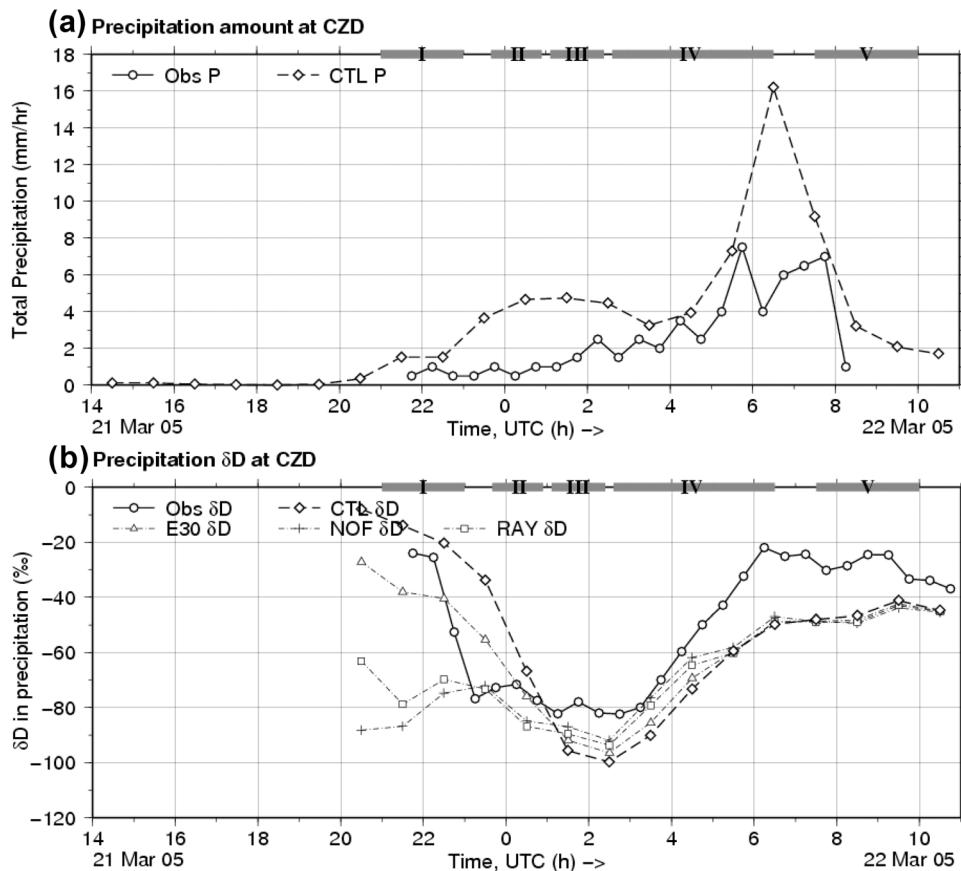


Figure 4. Simulated and observed time series of (a) precipitation amount and (b) isotopic composition in precipitation at CZD (38.61°N, 123.22°W). Note that all sensitivity experiments have identical precipitation amounts, but different isotopic compositions. Horizontal gray bars I–V on top axis indicate the periods of distinctive isotopic changes used in the analyses.

variances in the simulated precipitation isotopes. E30 shows the most similar isotopic variations to CTL but does not show a huge drop at the beginning of the event. Neither NOF nor RAY showed the enrichment at the beginning of the precipitation. Overall, CTL shows the best skill in reproducing observed variations in δD .

[25] It is also worthwhile to mention that the difference between CTL and E30 is less apparent than the difference between E30 and NOF. This indicates a lower sensitivity of the equilibrium fraction factor ε when the fraction is larger, in other words, when the impact of the kinetic isotopic exchange is more strongly taken into account. As Lee and Fung [2008] estimated from theoretical equations, the real fraction of equilibrium varies by meteorological condition, layer thickness, falling droplet size, and model time step, and $\varepsilon = 95\%$ for large-scale condensation tends to be an overestimation. Our experiments suggest that consideration of the kinetic isotopic exchange is primarily important to simulate the variation of δD in precipitation, but the equilibrium fraction factor above 30% is not that sensitive in this case.

3.3. Condensation at Different Levels and Its Contribution to Rainfall

[26] In this section C08's conclusion is reexamined using the model simulation data. Figure 5 displays the modeled

contribution of condensation at different levels during the five periods: the beginning enrichment phase (I), sudden-drop phase (II), depletion phase (III), increase phase (IV), and ending enrichment phase (V). The amounts of condensation and evaporation at all 28 σ levels were recorded every 20 s, and the total contributions to ground precipitation at each level were calculated. For easier viewing the contributions from similar levels were summed, and only seven vertical categories are shown in Figure 5.

[27] Figure 5 clearly illustrates temporal changes of level where condensation took place. In period I the lowermost level that positively contributed (condensation in total) to the precipitation at the surface is around 800 hPa (2 km MSL). Layers below this level were diagnosed as below the cloud base, and a total of 17% of precipitation evaporated from falling droplets in these layers. Above the cloud base the contributions are 50% each from 800 to 700 hPa and from 700 to 500 hPa, and a total of about 17% of the precipitation came from the layers above 500 hPa. Note that all of the condensation from levels above about 800 hPa was made in ice form. In period II the cloud base descended to 880 hPa (1.3 km MSL), and consequently, a greater contribution (11%) from the bottom part of the cloud (880 to 800 hPa levels) and less evaporation (3%) occurred below the cloud base (surface to 880 hPa) (figure not shown). In period III, the depletion phase of precipitation isotopic

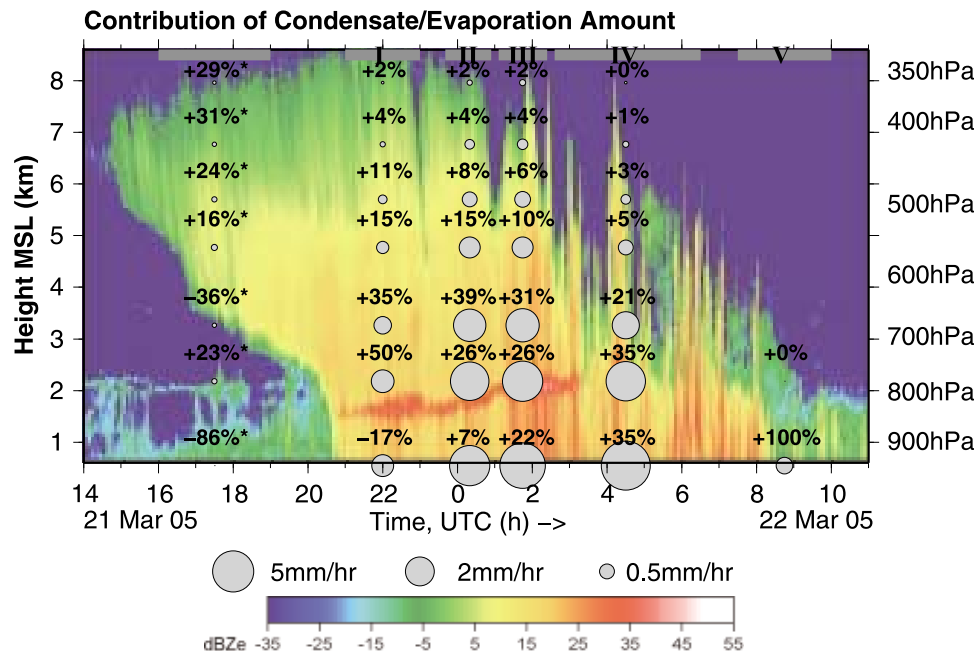


Figure 5. Contribution of condensation and evaporation relative to surface precipitation (percentages) and averaged precipitation rate (relative size of shaded circles) in the simulation for the periods indicated by horizontal gray bars I–V on the top axis. Numbers in the leftmost column (followed by asterisks) are relative to the precipitation rate at the 550 hPa level. The background image is Figure 3a of C08, the vertical Doppler radar reflectivity factor, but with the opposite time direction. MSL, mean sea level.

composition, the cloud base dropped further, to 940 hPa level (0.5 km MSL). The contribution from the bottom part of the cloud (i.e., 940 to 800 hPa levels) increased to more than 22%, and almost no evaporation occurred below the cloud base because the lower layers were already near saturation owing to the evaporation in the previous phases and because there was an additional supply of water vapor from the AR. Corresponding to the increased contribution from the bottom of the cloud, the contribution from the mid-troposphere (800 to 500 hPa levels) decreased to about 67% in total.

[28] In period IV, the enrichment phase, the contribution from the lower troposphere (surface to 800 hPa levels) increased to nearly 35%, and those from the midtroposphere (800 to 500 hPa) and upper troposphere (500 hPa and upper) decreased to about 61% and 4%, respectively. Particularly, the contribution from heights above 700 hPa decreased to 30%, owing to the descent of the cloud top. This is also noticeable from the observation of the vertical Doppler radar shown in the background of Figure 5. During period V, the end of the rain event and enrichment phase, almost all the precipitation was a result of condensation below the 800 hPa level. In this phase the precipitation type changed to convection for the first time during the whole rain event. The amount of precipitation from large-scale condensation was much less compared to that in other periods.

[29] An additional period, 1600 to 1900 UTC, on 21 March is shown in Figure 5 for the time just before the precipitation event, since the Doppler radar observation showed a remarkable descent of the precipitation area during this period. Note that the contribution percentages

for this period are calculated relative to the precipitation rate at the 550 hPa level due to zero precipitation at the surface, and the condensation amounts are very small compared to those in the other periods.

[30] In the *pre*-precipitation period (1600–1900 UTC), almost all condensation occurred above 5 km, and the condensation evaporated completely away in the lower parts. During periods I–III, rainfall was simulated at all levels up to 8 km. In periods IV and V there was almost no rainfall higher than 6 and 2 km, respectively. All of the simulated precipitation corresponded reasonably well with the Doppler radar observations. Although less noticeable in Figure 5, a close inspection of the original data for Figure 5 indicates a strong tendency for the proportions of precipitation to derive from condensation in and below the “bright band” (red horizontal band in the background image of Figure 5) in the radar returns, where frozen micrometeors melted and merged into liquid droplets, to increase as the bright band and the microphysical processes therein strengthened. Thus, although the comparisons are necessarily qualitative, these matches support the credibility of the simulation quality with respect to the profiles of condensation and evaporation affecting isotopic compositions. These simulated condensation–evaporation profiles were not modified in the sensitivity experiments, the results of which are described in the following section.

[31] From the model simulation the rapid change in the level of condensation from the lower warm part at the very beginning (period I) to the higher cold part in the middle of the event (period III), as hypothesized in C08, did not seem to occur. In fact, the contribution from the lower part increased significantly during the earlier phase. The biggest

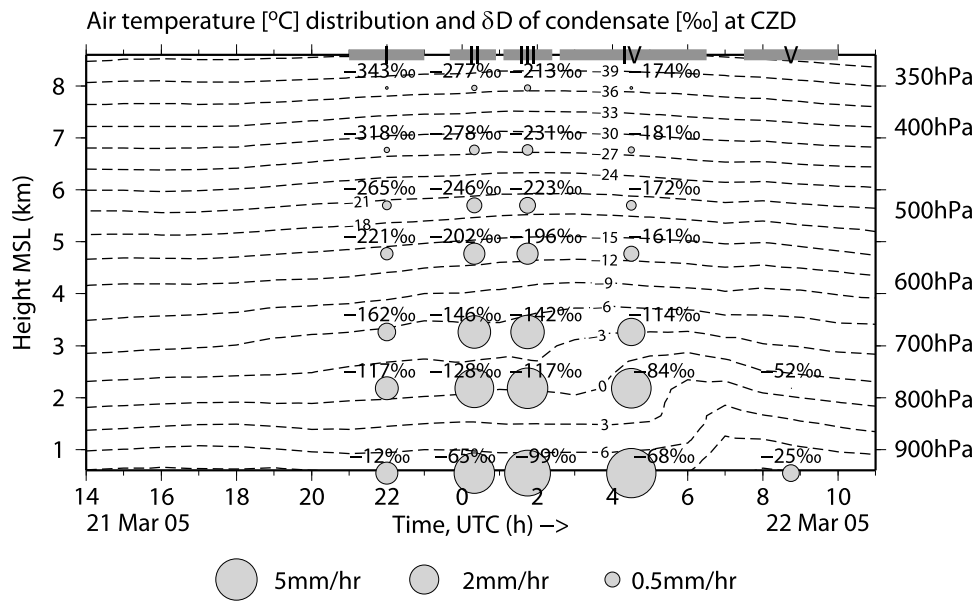


Figure 6. Temporal variation of air temperature vertical profiles (dashed contours) at CZD and mean δD of condensate (i.e., rain or ice droplets) during the five periods, indicated by horizontal gray bars on top axis (numbers beside shaded circles). Droplets (shaded circles) are the same as those in Figure 5.

difference with regard to the isotope variation between period I and period III is the existence of below-cloud evaporation in period I. By incorporating the kinetic isotopic exchange during below-cloud evaporation from droplets in the CTL experiment (see Figure 4b), the isotopic enrichment at the beginning of the event and the subsequent sudden depletion were well simulated. All the other experiments that excluded or lowered this effect failed to reproduce the rapid drop in δD , as discussed in the following subsection.

[32] Furthermore, Figure 6 displays temporal variations of temperature profiles. The conclusion from C08 suggested that the high- δD precipitation during periods I and V was the result of warm-temperature condensation near the surface (about 10°C) and the low- δD precipitation during period III was a result of cold-temperature condensation near the bright band (below 0°C). From the temperature profiles (Figure 6) and the condensation-evaporation profiles (Figure 5), it is very difficult to confirm that the warm surface vapor contributed to the precipitation during period I. Indeed, we averaged the air temperature with a weight of the condensation contribution amount as an indicator of averaged condensation temperature, and the results were -12° , -5° , and 12°C for periods I, III, and V, respectively, which clearly reflects that the average height of contribution only descended during the precipitation events.

[33] Also in Figure 6, weighted average δD values of condensate for periods I–V at representative heights are shown. From these values it is apparent that the δD of condensate at very high altitudes (e.g., 8 km level) keeps increasing, whereas at the surface it first decreases, then increases. This increasing tendency remains down to the 3 km level, with a smaller magnitude, but the tendency is suddenly disturbed below the 2 km level. More precisely, a large degree of enrichment in deuterium ($+105\%$ in δD) occurs from the 2 km level to the surface during period I,

and this enrichment lessens in the later periods ($+63\%$ for period II and $+18\%$ for period III). It is interesting to note that the condensates at the 2 km level for periods I–III coincidentally have similar isotopic compositions (-117% , -128% , and -117% , respectively), but owing to the near-surface processes, particularly droplet evaporation and kinetic isotopic exchange, the quite remarkable isotopic variation in precipitation appears. It can therefore be argued that there is no temperature effect (no signal of temperature-dependent fractionation) in surface precipitation isotopic composition within a single synoptic-scale event. Even though the temperature effect exists at the upper levels, it is overridden by the stronger isotopic processes near the surface. The temperature effect in precipitation emerges over longer time averages, partly as a result of background temperature differences between synoptic-scale events.

3.4. Isotopic Impact of Below-Cloud Evaporation

[34] Now we would like to return to Figure 4b and investigate why the kinetic isotopic exchange influences the isotopic variations of precipitation significantly at the beginning of the event, that is, the reason for the high δD value in period I. As already noted, the CTL experiment best reproduced the observed isotopic variation. The experiments with no (NOF) and less (E30) kinetic isotopic exchange between the falling droplets and the ambient humid air failed to simulate a high δD value during the first phase. Having a simple Rayleigh-type isotopic fractionation for evaporation also did not produce the correct enrichment.

[35] Figure 7a shows water vapor isotopic compositions at a low level (925 hPa) in these experiments. In the CTL the vapor δD suddenly dropped at about 2300 UTC on 21 March, similarly to the precipitation isotopes. The degree of the drop was less in E30, and there was almost

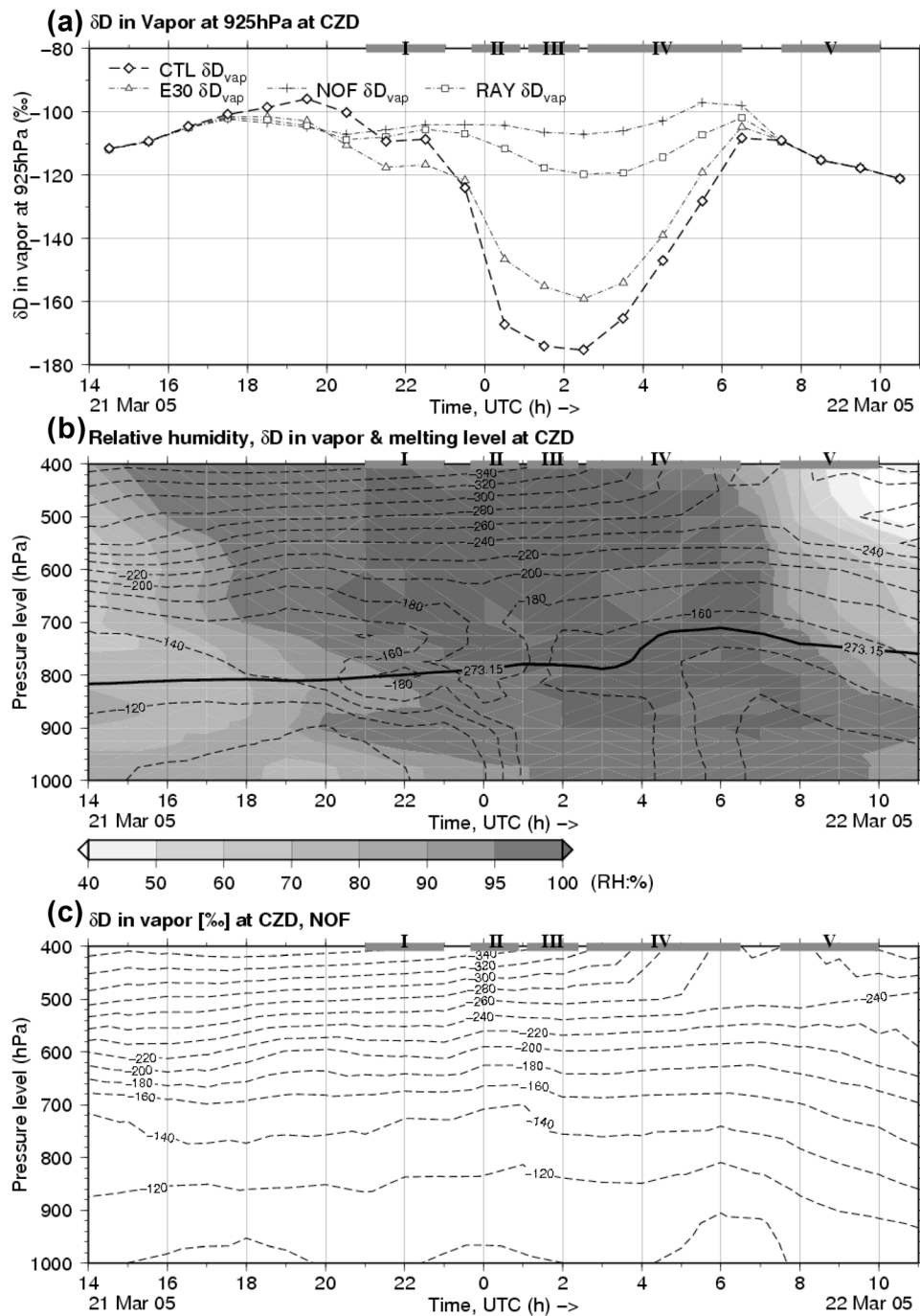


Figure 7. Time series of (a) the isotopic composition (δD) of vapor at the 925 hPa level and of (b) vertical profiles of relative humidity (shading), (b) melting level (bold solid line), and (b, c) isotopic composition (δD) of vapor (dashed contours) at CZD. The four sensitivity experiments are included in Figure 7a, but only the results from (control) CTL and NOF are shown in Figures 7b and 7c, respectively.

no drop in NOF and RAY. In NOF the iced condensation kept its isotopic composition when it fell below the cloud base. Therefore the precipitation at the surface had a more negative δD value. The nonfractionation evaporation from the falling droplets was not isotopically influential on the below-cloud water vapor.

[36] In the CTL the precipitation was more enriched in deuterium at the surface, owing to the kinetic isotopic exchange and the raindrop evaporation. The isotopic exchange made the relationship between the isotopic compositions of the droplets and the ambient, very humid air nearly reach the equilibrium state, as already introduced in

equation (2). Thus the isotopic composition in the ambient vapor, R_v , is introduced as follows:

$$R_v \approx \left(1 - (1 - f + \varepsilon\alpha_e f) \frac{m_0}{q}\right) R_{v0} + (1 - f + \varepsilon f) \frac{m_0}{q} R_{r0}, \quad (3)$$

$$\Delta R_v \equiv R_v - R_{v0} = -(1 - f + \varepsilon\alpha_e f) \frac{m_0}{q} R_{v0} + (1 - f + \varepsilon f) \frac{m_0}{q} R_{r0}, \quad (4)$$

where $f = m/m_0$, that is, the remaining ratio of the droplets after evaporation. Therefore, the tendency of the vapor isotope composition depends on the relative relationship between R_{r0} and R_{v0} , such as

$$\Delta R_v < 0, \quad \text{when} \quad R_{r0} < \frac{1 - f + \varepsilon\alpha_e f}{1 - f + \varepsilon f} R_{v0}. \quad (5)$$

Equation (5) describes that when falling droplets from the upper level have a lower isotopic composition than a threshold value, $\frac{1 - f + \varepsilon\alpha_e f}{1 - f + \varepsilon f} R_{v0}$, the vapor isotopic composition decreases. Since the isotopic composition of vapor is usually lower at higher altitudes, the falling droplet tends to have a lower isotopic composition than the threshold.

[37] The degree of the decrease in the vapor isotopic composition depends on the remaining ratio of droplets f , the rate of reaching the equilibrium state ε , and the existing ratio of droplets in vapor m_0/q , when R_{v0} and R_{r0} are fixed as shown in equation (4). Note that f is negatively correlated with the evaporation rate from droplets and m_0/q is almost equivalent to the precipitation rate. Isotopic depletion of water vapor is maximum when $f = 1$ (no change in raindrop mass) and $\varepsilon = 1$ (perfect equilibrium), and it is proportional to m_0/q (correlated with precipitation rate). The last relationship is partly responsible for the ‘‘amount effect,’’ which is a negative correlation between precipitation amount and precipitation isotope ratio. As *Lee and Fung* [2008] summarized, the amount effect is a cumulative consequence of multiple processes. The process given here describes a rather short-term (within a single event) relationship between isotopes and precipitation amount.

[38] Figure 7b indicates that the relative humidity (shaded) near the surface was less than 90% during period I, so that droplet evaporation is expected to be greater (Figure 5), and consequently, the precipitation rate should be low (Figure 4b). In this case the depletion of heavy isotopes in water vapor was not significant, as described in the previous paragraph (both f and m_0/q are small). However, in period II the air humidity reached almost 100%, owing to the strong advection of humid air associated with the AR toward the location, as well as to the droplet evaporation during the previous phase. Then the evaporation rate became almost 0 (so that f approached 1) and the precipitation rate became higher (so that m_0/q became larger). In this case, the isotope ratio of vapor below 800 hPa started to decrease. The depletion continued until R_{r0} approached $\alpha_e R_{v0}$, where the falling droplets were already in the isotopic equilibrium state with the ambient vapor, implying that there was little vertical gradient in the vapor isotopic profile.

[39] Figure 7b also shows the temporal variations of the vertical profiles of the water vapor δD . The water vapor δD

at levels lower than 850 hPa (where liquid condensate existed) decreased rapidly from about 2300 UTC on 21 March, until there was almost no vertical gradient in δD (period II). There was no additional decrease while there was little vertical gradient during 0100 to 0230 UTC on 22 March (period III). An increase occurred during period IV, possibly for a different reason, as described in the next section.

[40] In Figure 7c the vertical profiles of vapor δD in NOF are shown as a contrast to those in CTL (Figure 7b). It can clearly be seen that the kinetic isotopic exchange associated with droplet evaporation generates large isotopic variations in vapor at levels below 700 hPa. Without consideration of this impact, the isotopic vertical profile becomes more stable even when there is heavy AR rainfall during all five periods, particularly in the early stages (periods I–III).

3.5. Decomposition of the Contributors of the Isotopic Variations

[41] Figure 8 shows the accumulated contribution of model physical and dynamical processes on vapor δD for the five periods illustrated in Figures 4 and 5, at three heights. The calculation was done based on the output at every time step. The model’s physical processes (‘‘physics’’ hereafter) are so-called ‘‘physical parameterizations,’’ which include large-scale condensation, convective precipitation, planetary boundary layer mixing, and so on. The model’s dynamical processes (‘‘dynamics’’ hereafter) are strictly driven by the Eulerian equations of motion of a fluid.

[42] At $\sigma = 0.965$ (Figure 8a; at about the 940 hPa level), the largest contributor to the sudden drop in vapor δD during period II was the physical process, particularly kinetic isotopic exchange during the large-scale condensation. In contrast, the largest contributor to the increase in vapor δD during period IV was the dynamical process, that is, horizontal inflow of the deuterium-enriched water vapor from the upstream. The physical processes, namely, convection and large-scale condensation, contributed to the drop in vapor δD , but the dynamical advection was large enough to override the contribution of the physics during period IV.

[43] The situation was almost the same at the fifth level (Figure 8b; at about the 890 hPa level), but the negative contribution (making the vapor δD values more negative) of the physics and positive contribution (making the vapor δD values less negative) of the dynamics during period IV were both larger than those at lower levels. There were smaller isotopic changes at the seventh level (Figure 8c; around the 820 hPa level). The contributions owing to the physics and dynamics compensated each other and the isotopic compositions did not vary as much at this level. The main implication of the analysis here is that the rapid drop of the δD in water vapor at low levels was due to isotopic exchange and the increase in later phases was due to horizontal advection.

4. Summary and Conclusions

[44] In this paper a time series of isotopic composition in precipitation sampled at 30 minute intervals by C08 was revisited to study short-time-scale changes in isotopic composition. The precipitation event was associated with an AR event during 20 to 22 March 2005. Various other useful meteorological measurements took place over the Bay Area,

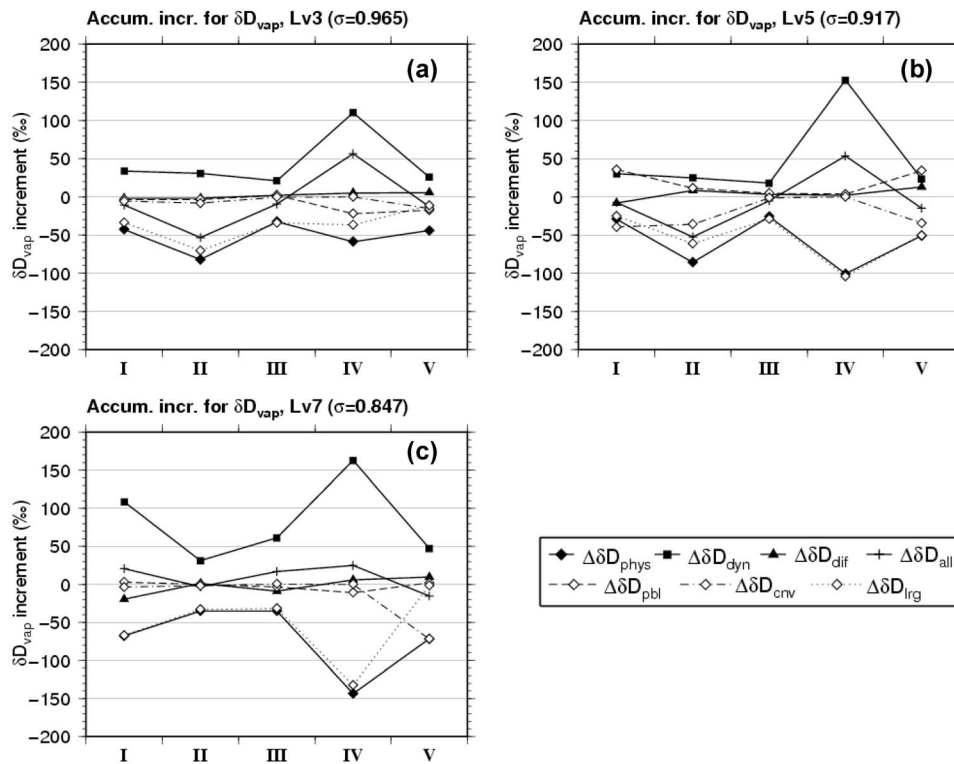


Figure 8. Accumulated increments in isotopic composition (δD) of vapor by different processes in the model at (a) 940 hPa, (b) 890 hPa, and (c) 820 hPa levels during the five isotopically distinct periods I–V. Processes are divided into three types, namely, physics (filled diamonds), dynamics (filled squares), and diffusion (filled triangles) processes. Total increments are also represented by lines with crosses. The impact from the physics process is further divided into the planetary boundary layer (dashed line), deep convection (dot-dashed line), and large-scale condensation (dotted line), and they are all denoted by open diamonds.

California. We developed a regional version of the isotope-incorporated AGCM, the IsoRSM, to simulate the meteorological and isotopic variations of this event.

[45] A set of experiments with the IsoRSM was conducted for this event. The experiments utilized a Reanalysis-“nudged” isotope-incorporated AGCM simulation data set, also known as IsoGSM data [Yoshimura *et al.*, 2008], as the lateral boundary condition and initial states. The control simulation simulated well the meteorological fields during the event in terms of precipitation, wind, and temperature. According to the model results, most precipitation was of the nonconvective type and was generated from the middle to upper levels in the troposphere at the very beginning of the rain event, but it gradually lowered as time passed. This contradicted what C08 inferred from the isotopic data. C08 argued that the contribution occurred at low levels at the beginning of the event but gradually moved upward as time passed.

[46] A set of sensitivity experiments revealed that the kinetic isotopic exchange between falling droplets and ambient vapor was mainly responsible for the initial enrichment and following rapid drop of the δD in precipitation. This impact has been rather well known since the study by Miyake *et al.* [1968], but it was not taken into account in C08 because the classic study instead focused on an arid condition. However, under humid conditions too, the isotopic exchange associated with evaporation from falling droplets occurred below the cloud base and enriched the

isotopic composition of precipitation. When the relative humidity reached almost 100% below the cloud base and the condensation rate also increased (corresponding to period II), the water vapor δD below the cloud base began to decrease. Consequently, the δD of lower tropospheric water vapor (below 800 hPa) dropped until there was little vertical gradient in the isotopic composition of the water vapor in the lower troposphere (800 hPa to surface) during period III. This is why the δD of precipitation at the surface also decreased rapidly. Afterward a sufficient amount of fresh moisture was supplied by dynamical advection in the lower troposphere, and the water vapor gradually became enriched in heavy isotopes despite the opposite contribution from the precipitation process. After passing the precipitation peak the cloud top began descending with a little precipitation, and both vapor and precipitation kept their isotopic enrichment high δD values until the end of the rain event. Thus, the observed variations in precipitation isotopes were well simulated by the IsoRSM.

[47] The results of this study are strongly dependent on the accuracy of the regional model. Although the mechanism of isotope variation in the model seems to be very reasonable and realistic, many uncertainties remain. The most crucial is the evaporation of precipitation in the model, which is formulated in a very simple manner, without taking detailed cloud physical processes into account. We would like to note that there is some supporting evidence of the

occurrence of evaporation from observations. Figure 3a in C08 indicates that the precipitation echo existed only at upper levels in the preprecipitation stage, together with less than 100% relative humidity at lower levels, which strongly suggests that the evaporation most likely occurred at low levels in the beginning phase of the precipitation event, as shown in Figure 5.

[48] Owing to the limited observations and model imperfections, it is very difficult to conclude which mechanisms dominate in the real atmosphere. It is therefore important to verify the model with other high-frequency observation data. There are several observation studies in which some degree of isotopic enrichment was observed at the beginning of a single rain event [e.g., Miyake *et al.*, 1968; Gedzelman *et al.*, 2003; Fudeyasu *et al.*, 2008]. Moreover, recent technical developments have enabled us to measure vapor isotopes continuously with a high frequency [e.g., Lee *et al.*, 2006]. These surface vapor measurements are just as important as high-frequency precipitation isotope data to further verify the model and understand the re-evaporation mechanism. In addition to more verification with observations, it is important to improve the model. One obvious flaw in our model is that condensed water falls to ground immediately. In reality, while condensed water remains in the air in the form of cloud water or ice, it advects and eventually falls to the ground or evaporates away. We still do not know the significance of predicting cloud water, ice particles, and their isotopes separately from vapor, but it may not be negligible and may be worth further study.

[49] **Acknowledgments.** Numerical simulations were performed with computing resources at The Center for Observations and Prediction at Scripps (COMPAS) and at TeraGrid. A part of this work was also funded by the California Energy Commission Public Interest Energy Research (PIER) program, which supports the California Climate Change Center (award MGC-04-04), and NOAA (grant NA17RJ1231). The views expressed herein are those of the authors and do not necessarily reflect the views of NOAA. Dr. Paul Neiman helped to create the Doppler radar reflection image. We would also like to acknowledge the encouragement provided by Dr. J. Roads at the beginning of this study. The assistance of Ms. D. Boomer in refining the writing is appreciated.

References

- Abe, O., S. Agata, M. Morimoto, M. Abe, K. Yoshimura, T. Hiyama, and N. Yoshida (2009), A 6.5-year continuous record of sea surface salinity and seawater isotopic composition at Harbor of Ishigaki Island, southwest Japan, *Isotopes Environ. Health Studies*, *45*, 247–258.
- Bony, S., C. Risi, and F. Vimeux (2008), Influence of convective processes on the isotopic composition ($\delta^{18}\text{O}$ and δD) of precipitation and water vapor in the tropics: 1. Radiative-convective equilibrium and Tropical Ocean-Global Atmosphere-Coupled Ocean-Atmosphere Response Experiment (TOGA-COARE) simulations, *J. Geophys. Res.*, *113*, D19305, doi:10.1029/2008JD009942.
- Chou, M.-D., and M. J. Suarez (1994), An efficient thermal infrared radiation parameterization for use in general circulation models, *NASA Tech. Rep. TM-1994-104606*, Series on Global Modeling and Data Assimilation, NASA, Houston, Tex.
- Clark, I., and P. Fritz (1997), *Environmental Isotopes in Hydrology*, Lewis, Boca Raton, Fla.
- Coplen, T. B., P. J. Neiman, A. B. White, J. M. Landwehr, F. M. Ralph, and M. D. Dettinger (2008), Extreme changes in stable hydrogen isotope and precipitation characteristics in a landfalling Pacific storm, *Geophys. Res. Lett.*, *35*, L21808, doi:10.1029/2008GL035481.
- Dansgaard, W. (1964), Stable isotopes in precipitation, *Tellus*, *16*, 436–468.
- Ehhalt, D., K. Knott, J. F. Nagel, and J. C. Vogel (1963), Deuterium and oxygen 18 in rain water, *J. Geophys. Res.*, *68*, 3775–3780.
- Ek, M. B., K. E. Mitchell, Y. Lin, E. Rogers, P. Grunmann, V. Koren, G. Gayno, and J. D. Tarpley (2003), Implementation of Noah land surface model advances in the National Centers for Environmental Prediction operational mesoscale Eta model, *J. Geophys. Res.*, *108*(D22), 8851, doi:10.1029/2002JD003296.
- Friedman, I., L. Machta, and R. Soller (1962), Water-vapor exchange between a water droplet and its environment, *J. Geophys. Res.*, *67*(7), 2761–2766, doi:10.1029/JZ067i007p02761.
- Frankenberg, C., K. Yoshimura, T. Warneke, I. Aben, A. Butz, N. Deutscher, D. Griffith, F. Hase, J. Notholt, M. Schneider, H. Schrijver, and T. Röckmann (2009), Dynamic processes governing the isotopic composition of water vapor as observed from space and ground, *Science*, *325*, 1374–1377, doi:10.1126/science.1173791.
- Fudeyasu, H., K. Ichiyangi, A. Sugimoto, K. Yoshimura, A. Ueta, M. D. Yamanaka, and K. Ozawa (2008), Isotope ratios of precipitation and water vapor observed in Typhoon Shanshan, *J. Geophys. Res.*, *113*, D12113, doi:10.1029/2007JD009313.
- Gat, J. R. (2000), Atmospheric water balance—The isotopic perspective, *Hydrol. Process.*, *14*, 1357–1369.
- Gedzelman, S. D., and R. Arnold (1994), Modeling the isotopic composition of precipitation, *J. Geophys. Res.*, *99*, 10,344–10,471.
- Gedzelman, S., J. Lawrence, J. Gamache, M. Balack, E. Hindman, R. Black, J. Dunion, H. Willoughby, and X. P. Zhang (2003), Probing hurricanes with stable isotopes of rain and water vapor, *Mon. Weather Rev.*, *131*, 1112–1127.
- Hoffmann, G., M. Werner, and M. Heimann (1998), The water isotope module of the ECHAM Atmospheric General Circulation Model—A study on timescales from days to several years, *J. Geophys. Res.*, *103*(D14), 16,871–16,896, doi:10.1029/98JD00423.
- Hong, S. Y., and H. L. Pan (1996), Nonlocal boundary layer vertical diffusion in a medium-range forecast model, *Mon. Weather Rev.*, *124*, 2322–2339.
- Jouzel, J., and L. Merlivat (1984), Deuterium and oxygen 18 in precipitation: Modeling of the isotopic effects during snow formation, *J. Geophys. Res.*, *87*(D7), 11,749–11,757, doi:10.1029/JD089iD07p11749.
- Kanamaru, H., and M. Kanamitsu (2007), Scale-selective bias correction in a downscaling of global analysis using a regional model, *Mon. Weather Rev.*, *135*, 334–350.
- Kanamitsu, M., and H. Kanamaru (2007), 57-Year California Reanalysis Downscaling at 10 km (CaRD10): Part 1. System detail and validation with observations, *J. Climate*, *20*, 5527–5552.
- Kanamitsu, M., W. Ebisuzaki, J. Woollen, J. Potter, and M. Fiorino (2002), NCEP/DOE AMIP-II Reanalysis (R-2), *Bull. Am. Meteorol. Soc.*, *83*, 1631–1643.
- Kanamitsu, M., H. Kanamaru, Y. Cui, and H. Juang (2005), Parallel implementation of the regional spectral atmospheric model, CEC Report CEC-500-2005-014, California Energy Commission, Sacramento.
- Kanamitsu, M., K. Yoshimura, Y.-B. Yhang, and S.-Y. Hong (2010), Errors of interannual variability and trend in dynamical downscaling of reanalysis, *J. Geophys. Res.*, doi:10.1029/2009JD013511, in press.
- Lee, J. E., and I. Fung (2008), “Amount effect” of water isotopes and quantitative analysis of post-condensation processes, *Hydrol. Process.*, *22*, 1–8.
- Lee, X. H., R. Smith, and J. Williams (2006), Water vapour $^{18}\text{O}/^{16}\text{O}$ isotope ratio in surface air in New England, USA, *Tellus*, *58B*, 293–304.
- Majoube, M. (1971a), Oxygen-18 and deuterium fractionation between water and steam (in French), *J. Chim. Phys. Phys. Chim. Biol.*, *68*, 1423–1436.
- Majoube, M. (1971b), Fractionation in O-18 between ice and water vapor (in French), *J. Chim. Phys. Phys. Chim. Biol.*, *68*, 625–636.
- Merlivat, L. (1978), Molecular diffusivities of H_2^{18}O , HD^{16}O and H_2^{16}O in gases, *J. Chim. Phys.*, *69*, 2864–2871.
- Merlivat, L., and J. Jouzel (1979), Global climatic interpretation of the deuterium oxygen 18 relationship for precipitation, *J. Geophys. Res.*, *84*(C8), 5029–5033, doi:10.1029/JC084iC08p05029.
- Miller, N. L., P. Duffy, D. Cayan, H. Hidalgo, J. Jin, H. Kanamaru, M. Kanamitsu, T. O’Brien, N. Schlegel, L. Sloan, M. Snyder, and K. Yoshimura (2009), An evaluation of simulated California climate using multiple dynamical and statistical downscaling techniques, CEC Report CEC-500-2009-017-F, California Energy Commission, Sacramento.
- Miyake, Y., O. Matsubaya, and C. Nishihara (1968), An isotopic study on meteoric precipitation, *Papers Meteorol. Geophys.*, *19*, 243–266.
- Moorthi, S., and M. J. Suarez (1992), Relaxed Arakawa-Schubert: A parameterization of moist convection for general circulation models, *Mon. Weather Rev.*, *120*, 978–1002.
- Ralph, F. M., P. J. Neiman, and G. A. Wick (2004), Satellite and CALJET aircraft observations of atmospheric rivers over the eastern North Pacific Ocean during the winter of 1997/98, *Mon. Weather Rev.*, *132*, 1721–1745.

- Rozanski, K., L. Araguas-Araguas, and R. Gonfiantini (1993), Isotopic patterns in modern global precipitation, in *Climate Change in Continental Isotopic Records*, Geophysical Monograph 78, pp. 1–36, edited by P. K. Swart, K. C. Lohmann, J. McKenzie, and S. Savin, American Geophysical Union, Washington D. C.
- Schneider, M., K. Yoshimura, F. Hase, and T. Blumenstock (2010), The ground-based FTIR network's potential for investigating the atmospheric water cycle, *Atmos. Chem. Phys.*, *10*, 3427–3442.
- Stewart, M. K. (1975), Stable isotope fractionation due to evaporation and isotopic exchange of falling water drops, *J. Geophys. Res.*, *80*(9), 1133–1146, doi:10.1029/JC080i009p01133.
- Sturm, K., G. Hoffmann, B. Langmann, and W. Stichler (2005), Simulation of d18O in precipitation by the regional circulation model REMOiso, *Hydrol. Process.*, *19*, 3425–3444, doi:10.1002/hyp.5979.
- Sturm, C., G. Hoffmann, and B. Langmann (2007), Simulation of the stable water isotopes in precipitation over South America: Comparing regional to global circulation models, *J. Climate*, *20*, 3730–3750.
- Uemura, R., Y. Matsui, K. Yoshimura, H. Motoyama, and N. Yoshida (2008), Evidence of deuterium excess in water vapour as an indicator of ocean surface conditions, *J. Geophys. Res.*, *113*, D19114, doi:10.1029/2008JD010209.
- Yoshimura, K., and M. Kanamitsu (2008), Dynamical global downscaling of global reanalysis, *Mon. Weather Rev.*, *136*, 2983–2998.
- Yoshimura, K., and M. Kanamitsu (2009), Specification of external forcing for regional model integrations, *Mon. Weather Rev.*, *137*, 1409–1421.
- Yoshimura, K., T. Oki, N. Ohte, and S. Kanae (2003), A quantitative analysis of short-term ¹⁸O variability with a Rayleigh-type isotope circulation model, *J. Geophys. Res.*, *108*(D20), 4647, doi:10.1029/2003JD003477.
- Yoshimura, K., T. Oki, and K. Ichiyangi (2004), Evaluation of two-dimensional atmospheric water circulation fields in reanalyses by using precipitation isotopes databases, *J. Geophys. Res.*, *109*, D20109, doi:10.1029/2004JD004764.
- Yoshimura, K., M. Kanamitsu, D. Noone, and T. Oki (2008), Historical isotope simulation using Reanalysis atmospheric data, *J. Geophys. Res.*, *113*, D19108, doi:10.1029/2008JD010074.
-
- M. Dettinger and M. Kanamitsu, Scripps Institution of Oceanography, University of California, San Diego, 8605 La Jolla Shores Dr., La Jolla, CA 92093, USA.
- K. Yoshimura (corresponding author), AORI, 5-1-5 Kashiwanoha, Kashiwa, Chiba 227-8568, Japan. (kei@aori.u-tokyo.ac.jp)